



HAL
open science

Effect of porous activated carbon particles soaked in cyclopentane on CP-hydrate formation in synthetic produced water

Rafik Mallek, Christelle Miqueu, Matthieu Jacob, Pascal Le Mélinaire, Christophe Dicharry

► To cite this version:

Rafik Mallek, Christelle Miqueu, Matthieu Jacob, Pascal Le Mélinaire, Christophe Dicharry. Effect of porous activated carbon particles soaked in cyclopentane on CP-hydrate formation in synthetic produced water. *Journal of Water Process Engineering*, 2020, 38, pp.101660 -. 10.1016/j.jwpe.2020.101660 . hal-03491346

HAL Id: hal-03491346

<https://hal.science/hal-03491346>

Submitted on 17 Oct 2022

HAL is a multi-disciplinary open access archive for the deposit and dissemination of scientific research documents, whether they are published or not. The documents may come from teaching and research institutions in France or abroad, or from public or private research centers.

L'archive ouverte pluridisciplinaire **HAL**, est destinée au dépôt et à la diffusion de documents scientifiques de niveau recherche, publiés ou non, émanant des établissements d'enseignement et de recherche français ou étrangers, des laboratoires publics ou privés.



Distributed under a Creative Commons Attribution - NonCommercial 4.0 International License

Effect of porous activated carbon particles soaked in cyclopentane on CP-hydrate formation in synthetic produced water

Rafik Mallek,¹ Christelle Miqueu,² Matthieu Jacob,³ Pascal Le Mélinaire,⁴ Christophe Dicharry^{1,*}

¹ *Université de Pau et des Pays de l'Adour, E2S UPPA, CNRS, TOTAL, UMR5150, Laboratoire des Fluides Complexes et leurs Réservoirs, Pau 64000, France.*

² *Université de Pau et des Pays de l'Adour, E2S UPPA, CNRS, TOTAL, UMR5150, Laboratoire des Fluides Complexes et leurs Réservoirs, Anglet 64600, France.*

³ *Pôle d'Etude et de Recherche de Lacq (PERL), TOTAL SA, 64170 Lacq, France.*

⁴ *BGH, Chemstart-up, 64170 Lacq, France.*

*Corresponding author(s): christophe.dicharry@univ-pau.fr (C. Dicharry)

ABSTRACT

Hydrate-based desalination (HBD) could be an interesting alternative to more conventional processes for desalinating high-salinity waters such as those produced during oil & gas extraction. The present study investigates the hydrate formation stage of a recently patented HBD process, in which porous activated carbon particles (PACP) are used as guest (here cyclopentane (CP)) reservoirs and carriers for hydrate formation. The effects of the CP content (0.5 to 1 g of CP per gram of PACP), of the PACP particle size (400 and 700 μm), the stirring rate (0 to 360 rpm), and the salinity of the synthetic produced water (3.5 to 16 wt% NaCl) on hydrate formation were investigated in batch reactor experiments. The results showed that the CP-soaked PACP drastically enhanced both the hydrate formation kinetics and the water-to-hydrate conversion, even in the case with the highest water salinity (16 wt% NaCl). The best compromise (high kinetics and conversion) was obtained with the largest particle diameter (700 μm) loaded with 0.8 g of CP per gram of PACP. Stirring increases the

initial formation kinetics but slightly reduces the final water-to-hydrate conversion, determined at the end of a 78h-experiment. This study demonstrates that using porous particles soaked in cyclopentane is a promising option for boosting hydrate formation in an HBD process for desalination of high-salinity waters.

Keywords: Water desalination, produced water, hydrate-based desalination process, cyclopentane hydrate.

Abbreviations

PW: Produced water

CP: Cyclopentane

PACP: Porous activated carbon particles

HBD: Hydrate-based desalination

WHC: Water-to-hydrate conversion (%)

$WHC_{th,max}$: Maximal theoretical water-to-hydrate conversion (%)

$R\dot{W}HC$: Relative water-to-hydrate conversion rate (%/h)

$RWHC$: Relative water-to-hydrate conversion (%)

$RWHC_f$: Final relative water-to-hydrate conversion (%)

GR: Growth rate (mm/min)

Nomenclature

nD: Refractive index measured at a wavelength of 589.3 nm

[NaCl]: Sodium chloride concentration (wt%)

t_{ind} : Induction time (h)

1 Introduction

The oil and gas industry handles large volumes of water (three barrels of water for one of oil [1]) which is produced as a byproduct during oil and gas extraction. Produced water (PW) generally contains many organic and inorganic compounds, including oil droplets, chemical additives and various salts at different concentrations. The TDS (total dissolved solids) of PW, which represents the total concentration of dissolved matters (inorganic salts and organic matter) in water, varies between 0.1 and 28.5 wt% depending on the nature of the reservoir and the resource produced [2]. Cha and Seol [3] reported an average TDS of 8.2 wt% for PW, calculated based on the 58,707 entries of a database of oil and gas fields provided by the United States Geological Survey (USGS). Produced water is either injected into disposal wells, reinjected into the producing reservoir (to sustain reservoir pressure), or discharged into surface water bodies (very often into seawater). Reinjection of PW is the preferred management option since it offers a dual benefit: enhanced oil production and a lesser environmental impact (mainly lower water consumption and a lower impact on surface water quality and related ecosystems). Reinjected and discharged PW can be desalinated to avoid possible compatibility issues with formation water, to enhance oil production [4] or to meet local regulations.

Nowadays, medium-salinity waters such as seawater (3.5 wt%) are generally treated using reverse osmosis processes, which have a high salt-removal efficiency (> 99%) and a relatively low production cost (0.45 – 0.92 USD/m³ water) [5]. However, desalting complex effluents such as PW using reverse osmosis requires heavy and costly pretreatment (coagulation, microfiltration, etc.) of the feed water, which must be free of solid particles, organic matter, oil, etc. to protect the membranes [6]. Moreover, reverse osmosis is reported as ineffective in desalinating water with a TDS greater than 4.3 wt% [7], a range in which PW is generally situated.

Hydrate-based desalination (HBD) processes could potentially be used to treat this type of water [3,8]. Once the hydrates have formed, the hydrate crystals are separated from the remaining brine solution, in which salts are concentrated. The separated crystals are then dissociated and desalinated water is obtained [5]. The slow kinetics of hydrate formation - very often due to the limited contact area between the water phase and the hydrate former (which generally has a very low solubility in water), thus limiting the mass transfer between the two phases - are considered as one of the main obstacles to the large-scale development of hydrate-based processes [5,9]. Hydrate formation can be promoted by mechanical stirring of the phases for example, but this increases energy consumption and costs, and/or by adding surfactants known to act as hydrate promoters [10], but their use induces additional costs and contaminates the desalinated water. In an attempt to overcome these issues, a new hydrate-based desalination process, called BGH's process in this paper, was recently developed and patented [11]. This process is based on the HBD concept, but with the added innovation of using porous activated carbon particles (PACP) soaked in cyclopentane (CP), which can form gas hydrates at atmospheric pressure.

There are few studies on HBD desalination using CP as guest or co-guest molecules in the literature [3,9,12–18]. The influence of added particles - mainly graphite, silica sand and activated carbon - on hydrate formation has been investigated in different contexts (water desalination, methane storage, flow assurance, etc.) [19,20]. Graphite and silica sand particles were found to promote hydrate formation kinetics [16,19,21], whereas activated carbon was reported to be a kinetic hydrate inhibitor [20] or promoter [19,21–24]. To the best of our knowledge, no study has ever used porous particles as both a reservoir and a carrier of the guest molecules for hydrate formation.

The present work is an experimental study of the effect of CP-soaked PACP on hydrate formation in synthetic PW. Sodium chloride (NaCl) is used as a model salt to prepare the PW.

This choice is justified by the fact that NaCl represents the highest salt fraction in real PW [2]. Effectively, referring to the USGS database, Cha and Seol reported that the average sodium chloride content in real PW is 70% higher than those of the other main mineral salts present [3]. This article does not look into the hydrate recovery and dissociation steps and focuses only on the hydrate formation stage of BGH's process. It investigates the effects of the presence of CP-soaked PACP, of the CP-loading rate of the PACP, of particle size, the stirring rate, and salinity on the hydrate formation kinetics and water-to-hydrate conversion. Prior to this though, preliminary experiments were performed without PACP to evaluate the thermodynamic and kinetic effects of NaCl on CP-hydrate formation.

2 MATERIALS AND METHODS

2.1 Materials and Apparatus

Cyclopentane (CP) (purity of 97%) was purchased from Sigma Aldrich. Deionized water (resistivity of 18.2 M Ω .cm) was produced by a Purelab laboratory water-purification system. Sodium chloride (NaCl) (purity of 99.5%) was supplied by Acros Organics. Two grades of porous activated carbon particles (PACP), G-BAC-G70R and A-BAC-SP, supplied by Keruha GmbH (Germany) were used in the hydrate formation experiments. According to the supplier, they have the same pore size distribution (PSD) and porosity, but different mean particle diameters (700 and 400 μ m respectively). Their particle size distributions are provided as supplementary material (Figure S1). Their specific surface area is between 1,100 and 1,300 m²/g. Plastic syringes (3-mL capacity) and cellulose acetate syringe filters (0.8- μ m mesh size), used to take and filter samples of the aqueous solution, were purchased from Sodipro. The amounts of NaCl required to prepare the PW were weighed using a precision balance with an uncertainty of \pm 0.001 g.

The effect of NaCl concentration on the CP-hydrate equilibrium temperature was studied using a set of glass flasks, each with a capacity of 30 mL, and two Julabo F32 cryostats using ethane-diol as a refrigerant fluid.

The effect of NaCl concentration on the hydrate growth rate at the water/CP interface was evaluated using a sealed cylindrical glass cell of 3 cm in diameter and with a capacity of 30 mL placed in a cylindrical metal-jacketed vessel, through which ethane-diol was circulated to control the temperature. The water/CP interface was observed using a binocular magnifier (Wild Heerbrugg) fitted with a CCD camera (IDS UI124xSE-C) and positioned above the glass cell. The cell was backlit by an LED light table (Edmund Optics). The snapshots of the interface were recorded on a PC at regular intervals using a lab-made program.

The experiments based on BGH's process were conducted in two similar jacketed glass reactors with a 1-L capacity (Figure 1). Each reactor was fitted with a mechanical stirrer with a 4-bladed glass double propeller-stirrer shaft. A Lauda cryostat (RE 1050 G), using a silicone oil (Kryo 51) as a refrigerant, was used to control the temperature inside the reactors. The reactor temperature, measured using a PT100 temperature sensor ($\pm 0.15^\circ\text{C}$ uncertainty), was recorded by a data logger and a computer at regular intervals. The reactors have several inlets and outlets: the former were used to introduce the products (brine, PACP) when preparing the hydrate formation experiment, and the latter to collect the brine samples for refractive index measurement during the experiment.

The refractive index n_D (at a wavelength of 589.3 nm) of the collected brine samples was measured using an Anton Paar refractometer (Abbemat 3200) with an accuracy of ± 0.0001 . The sample salinity was then deduced using a previously determined " $n_D - [\text{NaCl}]$ " calibration curve (see eq. 2 in the Procedures section).

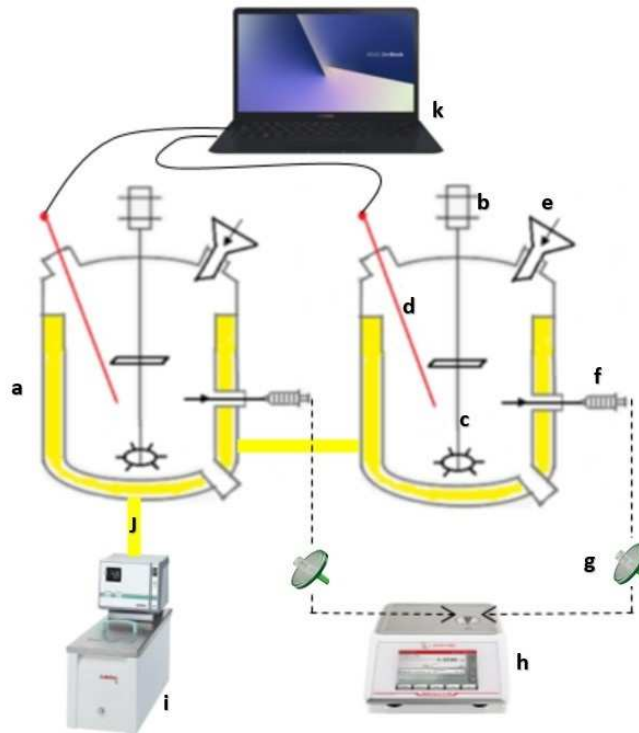


Figure 1. Experimental set-up for CP-hydrate formation: a) 1-L reactor, b) mechanical stirrer, c) stirring shaft, d) temperature sensor (PT100), e) funnel, f) syringe, g) syringe filter (0.8 μm), h) refractometer, i) cryostat, j) refrigerant fluid

2.2 Procedures

2.2.1 Preliminary investigation

The aim of the preliminary experiments without PACP was to analyze the effect of NaCl concentration on both the CP-hydrate equilibrium temperature and growth rate. Moreover, they served to choose the initial experimental conditions (initial water salinity; initial experimental temperature), referred to as the “starting points” in the chapters below, for testing BGH’s process.

2.2.1.1 Effect of NaCl concentration on the CP-hydrate equilibrium temperature

Fourteen flasks, each containing 2 g of CP, 18 g of water with different NaCl concentrations between 0 and 23 wt%, and a small rod (to help mix the fluids), were prepared, split into two concentration groups (group#1 (< 10 wt% NaCl) and group#2 (> 10 wt% NaCl)), and placed in two cryostats. Group#1 and group#2 were cooled down to -10°C and -22°C respectively and maintained at these temperatures for 24 hours to form ice. The ice was then melted by increasing the bath temperature to -4 and -18°C for group#1 and #2 respectively in order to trigger hydrate formation. The flasks were shaken manually at regular intervals over the course of 16 hours to promote the formation of CP hydrates. The bath temperature was then increased to 0 and -14°C for group#1 and #2 respectively. These temperatures were 1°C lower than the lowest CP-hydrate equilibrium temperatures at NaCl concentrations of 10 wt% and 23 wt% found in the literature [25–28].

The CP-hydrate equilibrium temperatures were determined using a “step-heating method” [29], which consists in applying a stepwise heating method combined with a sufficiently long equilibrium time at each step. In our experiments, the bath temperature was increased by steps of 0.2°C and maintained at the new temperature for 4 to 12 hours. The bath temperature was monitored using a PT100 probe ($\pm 0.15^\circ\text{C}$ uncertainty). The presence of CP hydrates in the flasks was visually checked at each step. If CP hydrates were still present, the flask was manually shaken before the next temperature increase. When only a small amount of CP hydrates remained, the temperature step was reduced to 0.1°C. The process was repeated until the last CP-hydrate crystals had melted. The CP-hydrate equilibrium temperatures were calculated as the arithmetic mean of the last two temperatures (before and after the last CP-hydrate crystals had melted). Any uncertainties regarding the measured equilibrium temperatures were evaluated as the sum of PT100 uncertainty ($\pm 0.15^\circ\text{C}$) and either $\pm 0.05^\circ\text{C}$,

for the temperature step of 0.1°C, or $\pm 0.1^\circ\text{C}$ if the CP-hydrate crystals had melted, before the temperature step was reduced from 0.2 to 0.1°C.

2.2.1.2 Effect of NaCl concentration on the CP-hydrate growth rate

Nine aqueous solutions with different NaCl concentrations (0, 1, 2, 3.5, 4, 6, 8, 10, and 16 wt%) were prepared. 20 mL of NaCl solution and 4 mL of CP were transferred to the cylindrical glass cell. The latter was placed in the metal-jacketed vessel and covered with a petri dish to limit CP evaporation. The temperature of the system was set such as to obtain the desired subcooling. Two different subcoolings (2°C and 6°C) were investigated: at 6°C, the lateral hydrate growth rates of all the different NaCl preparations were measured, whereas at 2°C, they were measured only for NaCl concentrations of 0, 3.5, 10, and 16 wt%. Hydrate crystallization was triggered by seeding the system with a few CP-hydrate crystals prepared beforehand. Because of their intermediate density, the seeds settled at the water/CP interface. The binocular magnifier was then focused on the crystals located on the flat part of the interface (around the vertical shaft of the cell). The lateral hydrate growth rate (GR) was evaluated by measuring the distance covered by the hydrate crystallization front at the water/CP interface in a given growth direction on two snapshots taken at different times. Three measurements were performed, each on a different point of the crystallization front, and the mean GR value was calculated. The GR uncertainty was calculated as the deviation from the mean GR value. The uncertainty of the imposed subcooling was $\pm 0.3^\circ\text{C}$.

2.2.2 Hydrate formation experiments in BGH's process

The study investigated the effects of the presence and absence of PACP at different stirring rates and, in the case of the system with PACP, the effect of the CP-loading rate, the PACP

size and water salinity on the CP-hydrate formation kinetics and the total amount of hydrates formed.

For this purpose, a series of experiments was carried out using the glass reactors. Synthetic water was first introduced into the reactors and cooled down to the experiment temperature. Stirring was started and set to the target rate (0, 180, or 360 rpm). Alongside that, CP - or PACP soaked in CP - were cooled in a freezer for 16 hours to -0.5°C and 0.5°C respectively, before being introduced into the reactors. This procedure was used to prevent hydrate crystallization before the system temperature reached the target experiment temperature. Note that, to avoid moisture crystallizing on the soaked PACP - which could trigger hydrate formation before the PACP were introduced into the reactors - they were not cooled to negative temperatures in the freezer. If they had been, it would have been impossible to evaluate the effect of PACP on induction time since hydrate formation would have been spontaneous.

The hydrate formation kinetics were quantified based on the induction time for hydrate crystallization t_{ind} and the relative water-to-hydrate conversion rate $R\dot{W}HC$ determined one hour after the onset of hydrate crystallization:

- t_{ind} was calculated as the time elapsed from the moment when CP or the soaked PACP were introduced into the reactor to the start of temperature increase due to hydrate crystallization. Note that when hydrate crystallization did not occur in the first two hours, it was triggered by seeding the system with a few CP-hydrate crystals prepared beforehand. Moreover, t_{ind} was measured only in the experiments where the effect of PACP and the stirring rate were investigated. In the other experiments, hydrate crystallization was systematically initiated by seeding the system with a few CP-hydrate crystals.

- $R\dot{W}HC$ was calculated as $R\dot{W}HC = \frac{100}{\Delta t} \Delta \frac{WHC}{WHC_{th,max}}$ where $\Delta t = 1\text{h}$ and WHC is the water-to-hydrate conversion, $WHC_{th,max}$ the maximum value of WHC that should be obtained,

either when all the CP initially present in the system is converted to hydrates or when the system reaches the CP-hydrate equilibrium curve (Figure 2). Note that in all the experiments of this study, water was in excess since the molar ratio of water to CP is 30:1, which is greater than the stoichiometric water to CP molar ratio for complete conversion to hydrate (17:1).

The amount of hydrates formed at time t was quantified through $RWHC = 100 \times \left(\frac{WHC}{WHC_{th,max}} \right)_t$, and the final amount of hydrates formed was quantified through $RWHC_f = 100 \times \left(\frac{WHC}{WHC_{th,max}} \right)_{t=t_f}$ where t_f is the time at which the experiment is stopped.

During the experiments, WHC was determined based on the difference between the initial water salinity $[NaCl]_{t_0}$ and the water salinity at time t $[NaCl]_t$ using Equation 1.

$$WHC = 100 - \frac{100 * [NaCl]_{t_0} * (100 - [NaCl]_t)}{(100 - [NaCl]_{t_0}) * [NaCl]_t} \quad (\text{Eq. 1})$$

$[NaCl]_t$ was obtained from the refractive index (nD) measurement of the NaCl solution sample collected at time t and using the following “nD – [NaCl]” calibration equation (Equation 2):

$$[NaCl] = 564.55 nD - 752.49 \quad (\text{Eq. 2})$$

The nD measurements were performed at 20°C. The samples collected were filtered to remove any suspended solids (hydrate crystals, PACP or impurities) before measuring nD. We checked that the use of filters and the solubility of CP in water (86 mg/L at 10°C [3]) did not impact the nD values obtained. A check was also run to make sure that NaCl did not adsorb on the PACP at the salinities used (3.5, 10, and 16 wt%).

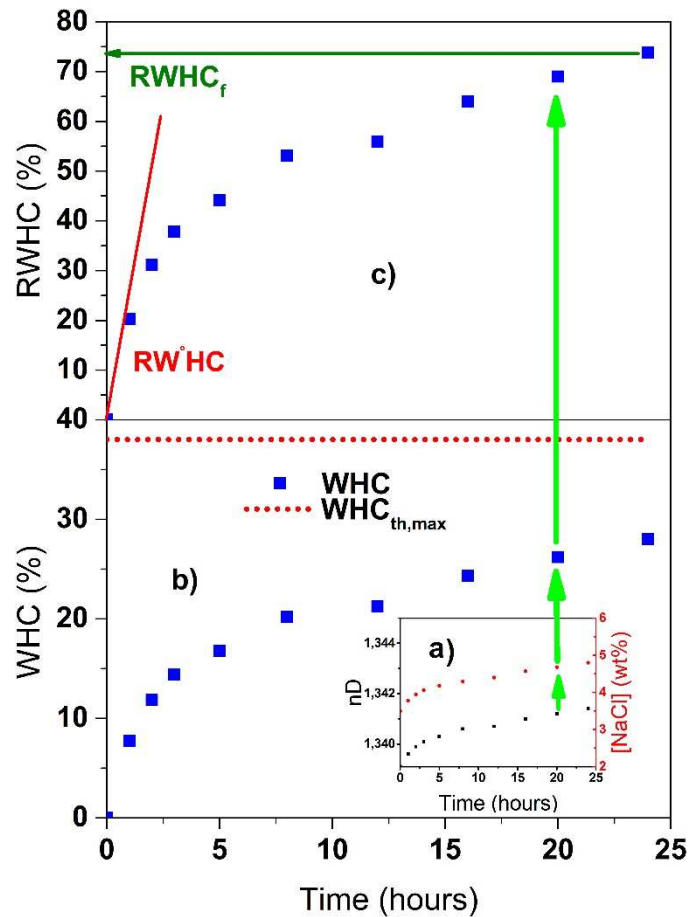


Figure 2. Experimental procedure to determine the relative water-to-hydrate conversion rate ($R\dot{W}HC$) and the final relative water-to-hydrate conversion rate ($RWHC_f$). a) Measured refractive index of the synthetic PW and deduced NaCl concentration vs. time (insert), b) calculated water-to-hydrate conversion (WHC) vs. time, c) determination of $R\dot{W}HC$ and $RWHC_f$

All the hydrate formation experiments performed in the glass reactor were duplicated. Consequently, each experimental point and value given in the corresponding figures and tables is the mean value of two experiments. The error bars in the figures and the uncertainties in the tables are calculated as the difference between the mean and minimum experimental values.

2.2.2.1 Effect of PACP and stirring rate on CP-hydrate formation

The CP-hydrate formation experiments - without and with G-BAC-G70R loaded with 0.8 g of CP per gram of PACP - were conducted at the starting point 1 (3.5 wt% NaCl; - 0.5°C) and at stirring rates of 0, 180, and 360 rpm for 78 hours. For these experiments, 777.2 g of a NaCl solution (750 g of deionized water and 27.2 g of NaCl) and 100 g of CP - or 125 g of PACP soaked in 100 g of CP - were introduced into each reactor where the temperature was set to - 0.5°C. Stirring started once the system temperature had reached the target temperature.

2.2.2.2 Effect of the CP-loading rate of PACP on CP-hydrate formation

The CP-hydrate formation experiments were conducted using G-BAC-G70R loaded with 0.5, 0.65, 0.8, and 1 g of CP per gram of PACP, at the starting point 1 (3.5 wt% NaCl; - 0.5°C) for 24 hours. 0.8 g of CP per gram of PACP was the loading rate typically used by the start-up BGH in its tests to work out its HBD process. Note that at this CP-loading rate, the particles were wet and stuck together, which suggests that both their pores and external surface were saturated with CP. The other loading rates used in the present study were chosen such as to evaluate the effect of this parameter on the hydrate formation kinetics and water-to-hydrate conversion over a range on either side of this value. For the CP-hydrate formation experiments, 777.2 g of a NaCl solution (750 g of deionized water and 27.2 g of NaCl) and 125 g of PACP soaked in 62.5, 81.25, 100 and 125 g of CP respectively were introduced into each reactor where the temperature was set to -0.5°C. A stirring rate of 180 rpm was used.

2.2.2.3 Effect of the size of PACP on CP-hydrate formation

The CP-hydrate formation experiments were conducted using G-BAC-G70R (mean particle diameter of 700 µm) and A-BAC-SP (mean particle diameter of 400 µm) loaded with 0.8 g of CP per gram of PACP, at the starting point 1 (3.5 wt% NaCl; - 0.5°C) for 24 hours. For these

experiments, 777.2 g of a NaCl solution (750 g of deionized water and 27.2 g of NaCl) and 125 g of PACP soaked in 100 g of CP were introduced into each reactor where the temperature was set to -0.5°C . A stirring rate of 180 rpm was used.

2.2.2.4 Effect of water salinity on CP-hydrate formation

In this part of the study, the CP-hydrate formation experiments were performed at two additional starting points defined as starting point 2 (10 wt% NaCl; -4.9°C) and starting point 3 (16 wt% NaCl; -9.5°C) for 24 hours. Although the operating points 1, 2 and 3 have different temperatures, they have the same initial subcooling of 6°C . The PACP used were G-BAC-G70R loaded with 0.8 g of CP per gram of PACP. A stirring rate of 180 rpm was used.

3 RESULTS AND DISCUSSION

3.1 Effect of NaCl on CP-hydrate formation

3.1.1 Effect of NaCl concentration on the CP-hydrate equilibrium temperature

The CP-hydrate equilibrium temperatures obtained at the different NaCl concentrations investigated (0 to 23 wt%) are plotted in Figure 3 and the measured values are given in Table 1. As expected, the increase in water salinity resulted in a decrease of the CP-hydrate equilibrium temperatures. Our experimental values are consistent with those published by Ho-Van et al. [25], Delroisse et al. [28], Zylyftari et al. [27] and Kishimoto et al. [26] (see Figure 3). More precisely, they range between the equilibrium points found in Ho-Van et al.'s study, determined by what they called rapid and slow processes. Ice equilibrium temperatures for the same range of NaCl concentrations are also shown in Figure 3. The starting points used for the hydrate formation experiments conducted in the glass reactors should be chosen in the region between the CP-hydrate and ice [30] curves.

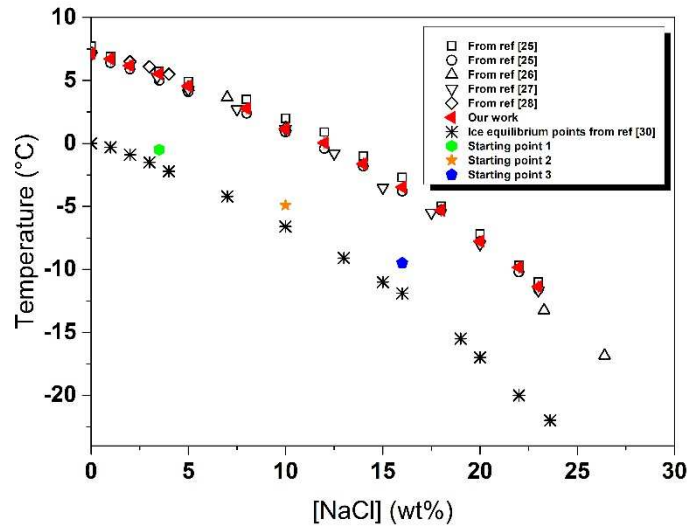


Figure 3. CP-hydrate and ice equilibrium temperatures as a function of NaCl concentration. This graph also shows the three initial experimental conditions (starting points 1, 2 and 3) used for the CP-hydrate formation experiments.

Table 1. CP-hydrate equilibrium temperatures (T_{eq}) measured at different NaCl concentrations ([NaCl])

[NaCl] ^a	0	1	2	3.5	5	8	10
(wt%)							
T_{eq} (°C)	7.13 ±	6.72 ±	6.18 ±	5.53 ±	4.56 ±	2.78 ±	1.15 ±
	0.20	0.20	0.25	0.19	0.26	0.24	0.21
[NaCl] ^a	12	14	16	18	20	22	23
(wt%)							
T_{eq} (°C)	-0.05 ±	-1.63 ±	-3.47 ±	-5.3 ±	-7.78 ±	-9.85 ±	-11.37 ±
	0.20	0.20	0.20	0.19	0.18	0.20	0.20

^a: ± 0.01 wt%

3.1.2 Effect of NaCl concentration on the CP-hydrate growth rate

In these experiments, CP-hydrate formation and growth occurred at the (quiescent) water/CP interface. A thin hydrate layer ended up covering the entire water/CP interface ($\sim 7.1 \text{ cm}^2$) available. Once the latter was totally covered, the hydrate growth stopped. Consequently, only a very small amount of hydrates formed in the system compared to the volume of NaCl solution (20 mL). This implies that the water salinity remained almost constant and that the imposed subcooling varied very little during hydrate formation. The measured lateral hydrate growth rate at the NaCl concentrations investigated (0 to 16 wt%) and the subcoolings of 2 and 6°C are shown in Figure 4. Images showing the morphology of the CP-hydrate crystals formed are provided as supplementary material (Figure S2). The CP-hydrate crystal morphology was found to depend essentially on the imposed subcooling. The lateral hydrate growth rate values obtained at these subcooling conditions are consistent with those measured by Kishimoto et al. [26] at around the same subcoolings.

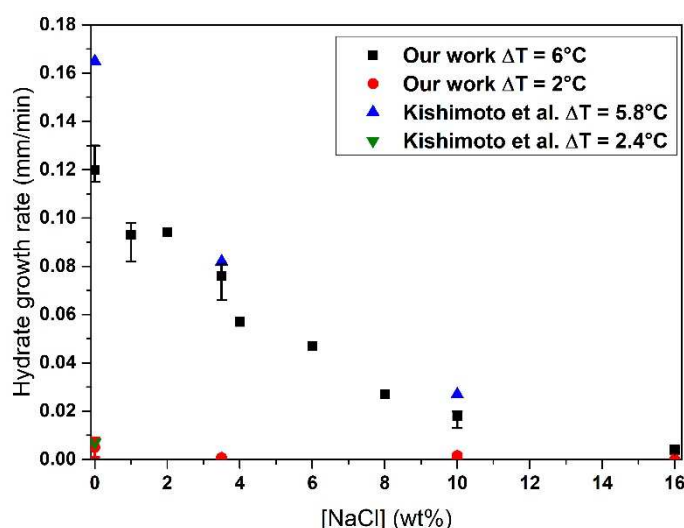


Figure 4. Measured lateral growth rate of CP-hydrates formed at the water/CP interface, at different NaCl concentrations and subcoolings of 2 and 6°C

We can see that both the NaCl concentration and the imposed subcooling drastically affect the hydrate growth rate. The latter decreases as the water salinity at a given subcooling increases and rises with the subcooling at a given salinity. The subcooling acts as a driving force and NaCl as a kinetic inhibitor for hydrate formation (in addition to its thermodynamic inhibitor effect (section 3.1.1)). According to the results shown in Figure 4, a high subcooling must be chosen to obtain a high hydrate growth rate in a hydrate-based desalination process. Consequently, in all the hydrate formation experiments performed, a subcooling of 6°C was chosen so that the system was deep inside the hydrate stability zone but remained outside the ice stability zone (see the three starting points in Figure 3). However, it is important to keep in mind that i) the introduction of the soaked PACP into the reactor, ii) the exothermicity of hydrate crystallization and, iii) the consumption of water molecules (by the growing hydrate phase) - which causes an increase in the salinity of the remaining liquid water and thus a decrease in the CP-hydrate equilibrium temperature - caused the subcooling to drop during the hydrate formation experiments. Considering these effects, we determined that the minimum subcoolings reached during the experiments performed at the starting points 1, 2 and 3 were 3.9, 4.1, and 5.1°C respectively. Note that the decrease in the imposed subcooling was mainly due to the exothermicity of the crystallization and the increase in salinity and not to the introduction of the soaked PACP into the reactor.

3.2 Hydrate formation experiments in BGH's process

3.2.1 Effect of PACP and the stirring rate on CP-hydrate formation

The effects of the absence and presence of PACP (G-BAC-G70R loaded with 0.8 g of CP per gram of PACP) and of the stirring rate on CP-hydrate formation are shown in Figure 5 and Table 2. For ease of comparison, data in Figure 5 are presented with a common base time $t =$

0, which corresponds to the onset of hydrate crystallization (whether the crystallization occurred spontaneously or had to be triggered by adding a few CP-hydrate crystals).

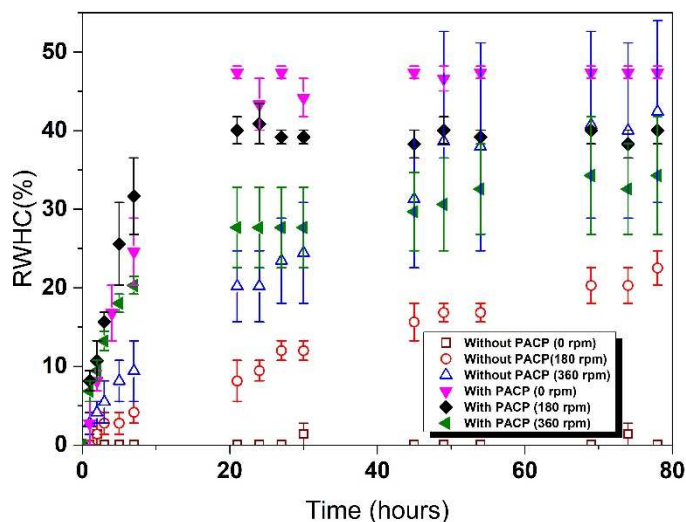


Figure 5. Effect of PACP (G-BAC-G70R loaded with 0.8 g of CP per gram of PACP) and the stirring rate on the relative water-to-hydrate conversion. The NaCl concentration is 3.5 wt%.

Table 2. Values of the induction time, the relative water-to-hydrate conversion rate and the final relative water-to-hydrate conversion (at $t = 78$ h) for the systems with and without PACP (G-BAC-G70R loaded with 0.8 g of CP per gram of PACP) and different stirring rates. The initial conditions for these experiments correspond to starting point 1 (Figure 3).

Stirring rate (rpm)	Without PACP						With PACP					
	0		180		360		0	180	360			
t_{ind} (h)	>2	>2	>2	>2	>2	>2	~0.02	>2	~0.02	>2	>2	>2
$R\dot{W}HC$ (%/h)	~0	~0	~0	~0	~0	~0	2.8 ± 2.8	8.2 ± 1.3	8.2 ± 1.3	6.8 ± 1.3	6.8 ± 1.3	6.8 ± 1.3
$RWHC_f$ (%)	~0	~0	~0	~0	~0	~0	47.4 ± 0.8	40.0 ± 1.7	40.0 ± 1.7	34.3 ± 7.5	34.3 ± 7.5	34.3 ± 7.5

For all the experiments performed without PACP, hydrate crystallization never occurred spontaneously in the first two hours the system spent at the target temperature of -0.5°C (i.e.

the induction time t_{ind} was greater than two hours). With PACP, t_{ind} lasted just a few minutes for one third of the experiments performed and more than 2 h for the others. The presence of PACP therefore increases the probability of early hydrate crystallization. The large number of nucleation sites provided by the PACP may explain this result. The stirring rates investigated do not affect the trend observed for t_{ind} .

$R\dot{W}HC$ is much higher for the system with PACP than without at a given stirring rate, and stirring increases $R\dot{W}HC$ in both systems. The increased contact area between water and CP, due either to the PACP (soaked in CP) or to the stirring of the system or both, can explain the trend observed. As expected, for the systems without PACP, a higher stirring rate ensures more efficient mixing of water and CP and thus a greater interface between the two phases. In the presence of PACP, the stirring causes dispersion of the particles, which tend to agglomerate in the water phase when no stirring is applied. However, in this case, the contact area between water and CP is predominantly controlled by the external specific surface area of the particles (in which CP is adsorbed), which does not vary with the agitation. This is why $R\dot{W}HC$ changes very little when the stirring rate is increased from 180 to 360 rpm.

$RWHC_f$ is much higher for the system with PACP than without at the stirring rates of 0 and 180 rpm. There is quite a spectacular difference in the $RWHC_f$ values obtained for the quiescent systems (0 rpm), where $RWHC_f$ is around 0 and 47.4% for the system without and with PACP respectively, 78 hours into the experiment. This is due to the difference in the size of the contact area between the water and the CP where hydrate formation and growth take place. Without PACP, the contact area is about 80 cm² (the cross-section of the glass reactor), whereas with PACP it is at least 11,000 cm² (the total external surface area of the particles). Moreover, the variation of $RWHC_f$ with the stirring rate displays an opposite trend according to whether or not PACP are present: $RWHC_f$ increases with the stirring rate in the systems without PACP and decreases in other cases. For the former, the increase in the contact area

between water and CP with stirring explains the trend observed. For the latter, the reason why $RWHC_f$ decreases as the stirring rate increases remains unclear. One of the reasons might be that the increase in the initial hydrate growth rate caused by the mixing leads to the early formation of an impermeable hydrate crust at the surface of the PACP, which limits (or stops) the hydrate formation process. Corak et al. [15] observed a similar tendency in their research on CP-hydrate formation in brines (3 wt% NaCl solutions). They reported that faster hydrate crystallization led to a greater amount of encapsulated CP and thus a smaller amount of hydrates (since the encapsulated CP is unavailable for hydrate formation).

An important finding in this section is that the CP-soaked PACP both increases the hydrate formation kinetics and “supplies” the hydrate reaction with CP. Note that the kinetic enhancement of hydrate formation observed in the presence of the PACP is consistent with the results reported by other authors for submillimetric particles, which were obtained mainly within the context of methane storage [21–24].

In the following sections, the effect of the PACP CP-loading rate, PACP size and water salinity on $R\dot{W}HC$ and $RWHC_f$ will be investigated. Because $RWHC$ remains almost constant for the systems with PACP after around 20 hours of experimentation (see Figure 5), 24 hours was chosen as the duration for all the following experiments. A stirring rate of 180 rpm was chosen to ensure homogeneity of the system during the experiments. Moreover, hydrate crystallization was triggered by seeding the system with a few CP-hydrate crystals.

3.2.2 Effect of the CP-loading rate of PACP on CP-hydrate formation

The effect of the CP-loading rate on CP-hydrate formation is illustrated in Figure 6, and the corresponding values of $R\dot{W}HC$ and $RWHC_f$ are given in Table 3.

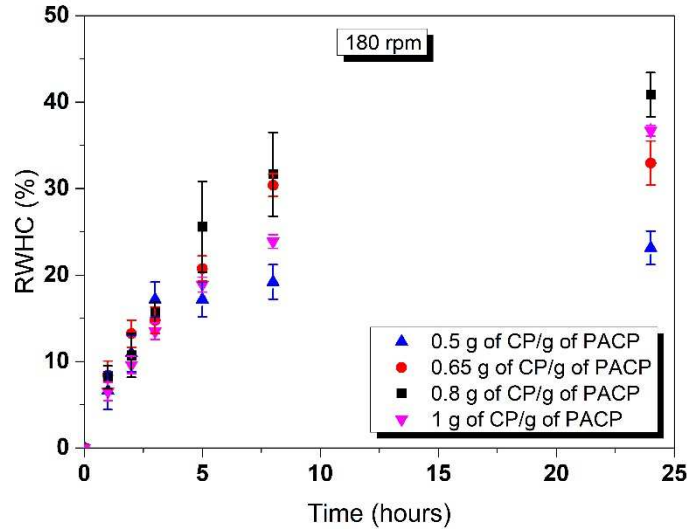


Figure 6. Effect of the CP-loading rate of PACP (G-BAC-G70R) on the relative water-to-hydrate conversion rate with 3.5 wt% NaCl. The stirring rate is 180 rpm.

Table 3. Values of the relative water-to-hydrate conversion rate and the final relative water-to-hydrate conversion (at $t = 24$ h) for the systems with PACP (G-BAC-G70R) at different CP-loading rates. The initial conditions for these experiments correspond to starting point 1 (see Figure 3). The stirring rate is 180 rpm.

CP-loading rate (gram of CP per gram of PACP)	0.5	0.65	0.8	1
$R\dot{W}HC$ (% / h)	6.6 ± 2.2	8.4 ± 1.6	8.2 ± 1.3	6.5 ± 1.1
$RWHC_f$ (%)	23.1 ± 1.9	33.0 ± 2.6	40.9 ± 2.6	36.7 ± 0.6

The $R\dot{W}HC$ points for the different CP-loading rates overlap for the first three hours of the experiment (Figure 6) meaning that $R\dot{W}HC$ hardly depends on CP-loading (Table 3). About five hours into the experiments, the variation rate of $R\dot{W}HC$ decreases for all the systems (Figure 6). At the end of the experiments (24 h), we can see that $RWHC_f$ significantly increases with the CP-loading rate when the latter is lower than or equal to 0.8 g of CP per

gram of PACP (Table 3). This can be explained by the increase in the amount of CP available for hydrate formation. However, a further increase in the CP-loading rate (to 1 g of CP per gram of PACP) causes $RWHC_f$ to drop. This decrease, due to the normalization of WHC, indicates a reduction in the ratio of the CP converted to hydrates to the CP present in the system. The main possible reason for this behavior is given below. When preparing the PACP, soaked in 1 g of CP per gram of PACP, some of the CP added was not adsorbed by the PACP but remained as a free liquid phase. Note that free liquid CP was not observed at the lower CP-loading rates used, which suggests that the maximum loading rate of PACP is approximately 0.8 g of CP per gram of PACP. When the PACP prepared with 1 g of CP per gram of PACP are added to the NaCl solution, the excess CP is dispersed as droplets in the bulk phase by agitation (180 rpm). Because the agitation used is not very vigorous, the increase in the water/CP interface caused by the excess CP in the bulk phase is small compared to the interface between the CP adsorbed in the PACP and the water. The amount of hydrates formed therefore increases less significantly than the amount of CP added, and $RWHC_f$ decreases as a consequence.

The results obtained in this section show that the optimal rate for loading PACP with CP in order to obtain high hydrate formation kinetics and conversion is around 0.8 g of CP per gram of PACP.

3.2.3 Effect of the size of PACP on CP-hydrate formation

The $RWHC$ values obtained for the 400- μm PACP (A-BAC-SP) were higher than those obtained with the 700- μm PACP (G-BAC-G70R) at the beginning of the hydrate formation experiment, but then became lower after about 5 hours (Figure 7). $R\dot{W}HC$ is therefore higher in the case of the smaller particles and $RWHC_f$ is higher in the case of the larger ones (Table 4). Because these PACP have the same PSD and the same porosity, the difference in the

$R\dot{W}HC$ obtained can probably be explained by the difference in the external specific surface area of the particles. Smaller particles effectively have a larger external specific surface area, which provides a higher water/CP contact area and more nucleation sites. Consequently, a higher hydrate growth rate can be expected. However, $R\dot{W}HC_f$ is higher when using 700- μm PACP, i.e. in the system with the PACP that offer the smaller water/CP contact area. A possible explanation might be that the slower initial hydrate growth rate ($R\dot{W}HC$) obtained with these PACP delays or limits the formation of an impermeable hydrate crust on the CP layer at the PACP surface. The CP transfer is sustained, and a greater amount of hydrates forms. Note that the trends observed here for the effect of the PACP size on $R\dot{W}HC$ are consistent with those reported by Li et al. in their study on the promotion effect of graphite on CP-hydrate formation [16]. The authors observed that the water-to-hydrate conversion was initially faster and then increased more slowly for the smallest particles than for the largest ones.

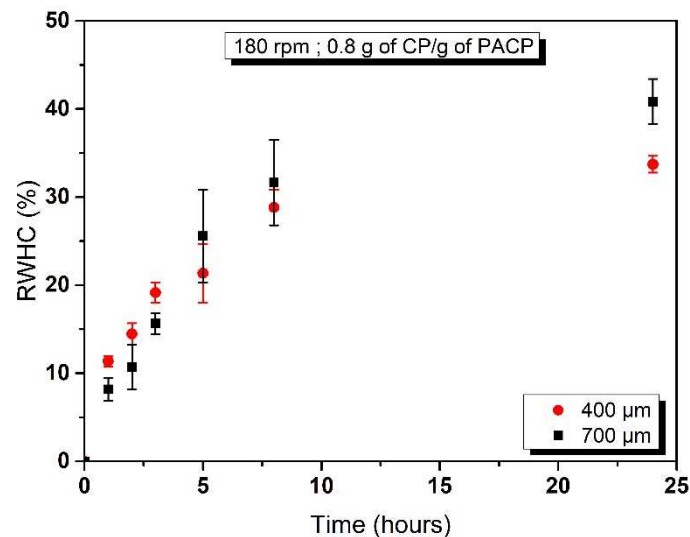


Figure 7. Effect of PACP size (400 and 700 μm) on the relative water-to-hydrate conversion with 3.5 wt% NaCl. The PACP are loaded with 0.8 g of CP per gram of PACP. The stirring rate is 180 rpm.

Table 4. Values of the relative water-to-hydrate conversion rate and the final relative water-to-hydrate conversion (at $t = 24$ h) for the different sizes of PACP (G-BAC-G70R (700 μm) and A-BAC-SP (400 μm)) loaded with 0.8 g of CP per gram of PACP. The initial conditions for these experiments correspond to starting point 1 (see Figure 3). The stirring rate is 180 rpm.

Particle size (μm)	400 (A-BAC-SP)	700 (G-BAC-G70R)
$R\dot{W}HC$ (%/h)	11.4 ± 0.6	8.2 ± 1.3
$RWHC_f$ (%)	33.7 ± 0.9	40.9 ± 2.6

3.2.4 Effect of water salinity on CP-hydrate formation

In Figure 8 and Table 5, the results of the CP-hydrate formation experiments conducted with the 700- μm PACP (loaded with 0.8 g of CP per gram of PACP) at concentrations of 10 and 16 wt% NaCl (starting points 2 and 3 in Figure 3) are shown and compared with those obtained in experiments using 3.5 wt% NaCl (given in paragraph 3.2.1).

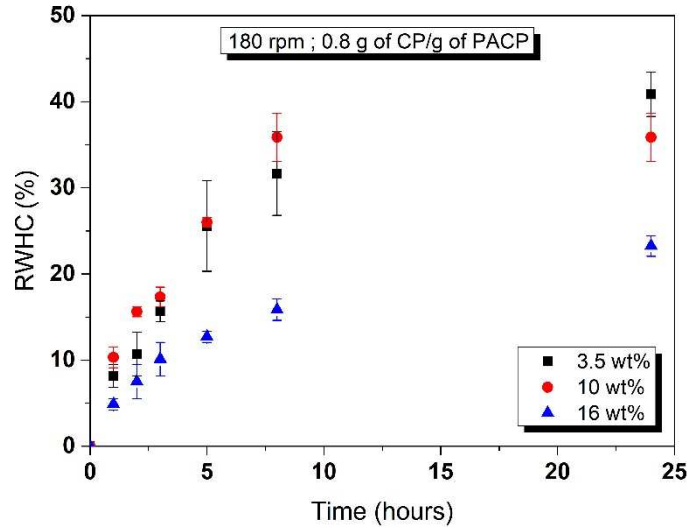


Figure 8. Effect of water salinity on the relative water-to-hydrate conversion. The PACP (G-BAC-G70R) are loaded with 0.8 g of CP per gram of PACP. The stirring rate is 180 rpm.

Table 5. Values of the relative water-to-hydrate conversion rate and the final relative water-to-hydrate conversion (at $t = 24$ h) for the system with PACP (G-BAC-G70R loaded with 0.8 g of CP per gram of PACP). The initial conditions for these experiments correspond to starting points 1, 2 and 3 (see Figure 3). The stirring rate is 180 rpm.

NaCl concentration (wt%)	3.5	10	16
$R\dot{W}HC$ (%/h)	8.2 ± 1.3	10.3 ± 1.2	4.9 ± 0.7
$RWHC_f$ (%)	40.9 ± 2.6	35.9 ± 2.8	23.3 ± 1.2

The $RWHC$ points obtained at time t for NaCl concentrations of 3.5 and 10 wt% are very similar (Figure 8). Consequently, $R\dot{W}HC$ and $RWHC_f$ have roughly the same values for both concentrations (Table 5). This very interesting result suggests that the PACP soaked in CP “cancel” the kinetic inhibition effect of NaCl (demonstrated in paragraph 3.1.2) for low to moderate salt concentrations. However, both $R\dot{W}HC$ and $RWHC_f$ significantly decrease in the system with 16 wt% NaCl. We saw in paragraph 3.1.2 that the kinetic inhibition effect of

NaCl on CP-hydrate formation is much stronger with 16 wt% NaCl than with 3.5 and 10 wt% NaCl. In actual fact, the hydrate growth rate (measured at the water/CP interface) with 16 wt% NaCl was 5 times lower than the growth rate with 10 wt% NaCl and 19 times lower than the one with 3.5 wt%. We can therefore infer that above a certain salinity, the presence of PACP is no longer able to “cancel” the kinetic inhibition effect of NaCl.

In their work on the desalination of PW using natural gas hydrates, Fakharian et al. [8] did not observe any hydrate formation in waters with a TDS higher than 160 g/L (i.e. 13.7 wt% of salts). In the present study, we succeeded in forming hydrates in water with 16 wt% NaCl. This illustrates another beneficial effect of using PACP soaked in CP.

4 Conclusion

This study demonstrates that using PACP soaked in CP significantly enhances hydrate formation kinetics and water-to-hydrate conversion. So, they act both as a kinetic promoter and a CP reservoir for hydrate formation. Combining PACP and stirring increases the formation kinetics but unexpectedly reduces the final water-to-hydrate conversion. The formation kinetics and water-to-hydrate conversion increase with the CP-loading rate of the PACP and then level off (or even slightly decrease) above a given loading rate (0.8 g CP per gram of PACP in our case). It was found that the smaller PAC particles induce higher hydrate formation kinetics but a lower final conversion. It is interesting to note that the use of PACP soaked in CP makes it possible to overcome the kinetic inhibition effect of NaCl for salinities of up to 10 wt%. Above this value, PACP still enhance hydrate formation but both the formation kinetics and the conversion decrease (compared to lower salinities).

BGH's process, which cleverly combines the use of a guest molecule (CP) forming hydrates at atmospheric pressure, and guest-soaked porous particles that promote hydrate formation and growth, appears as a promising desalination method. Nevertheless, the final water-to-

hydrate conversion needs to be improved since more than one half of the CP adsorbed in the PACP is not converted to hydrates (see Tables 2 and 5). Possible reasons for this behavior might be the formation of an impermeable hydrate layer on the PACP surface that blocks the contact between CP and water, and/or a fraction of CP tightly trapped in the pores of the PACP making it unavailable for hydrate formation. Further enhancement of the hydrate formation kinetics would also be advantageous in view of an industrial application of this desalination process. These points are currently under investigation.

Acknowledgements

This research was financially supported by Total. The authors would like to thank Frédéric Plantier and Manuel Ildefonso (UPPA), and Patrick Baldoni-Andrey, Hervé Nabet, and Stéphane Nowe (Total) for their valuable scientific input and discussions. Joseph Diaz (UPPA) is gratefully acknowledged for his technical assistance. Christelle Miqueu would like to acknowledge the E2S UPPA hub “Newpores” supported by the French *Investissements d'Avenir* program managed by the ANR (ANR-16-IDEX-0002).

References

- [1] R. Abousnina, An overview on oil contaminated sand and its engineering applications, *Int. J. Geomate* 10 (2015) 1615–1622. <https://doi.org/10.21660/2016.19.150602>.
- [2] K.L. Benko, J.E. Drewes, Produced water in the Western United States: Geographical distribution, occurrence, and composition, *Environ. Eng. Sci.* 25 (2008) 239–246. <https://doi.org/10.1089/ees.2007.0026>.
- [3] J.H. Cha, Y. Seol, Increasing gas hydrate formation temperature for desalination of high salinity produced water with secondary guests, *ACS Sustain. Chem. Eng.* 1 (2013) 1218–1224. <https://doi.org/10.1021/sc400160u>.

- [4] R.R. Nair, E. Protasova, S. Strand, T. Bilstad, Membrane performance analysis for smart water production for enhanced oil recovery in carbonate and sandstone reservoirs, *Energ. Fuel* 32 (2018) 4988–4995. <https://doi.org/10.1021/acs.energyfuels.8b00447>.
- [5] P. Babu, A. Nambiar, T. He, I.A. Karimi, J.D. Lee, P. Englezo, P. Linga, A Review of clathrate hydrate based desalination to strengthen energy–water nexus, *ACS Sustain. Chem. Eng.* 6 (2018) 8093–8107. <https://doi.org/10.1021/acssuschemeng.8b01616>.
- [6] M. Çakmakce, N. Kayaalp, I. Koyuncu, Desalination of produced water from oil production fields by membrane processes, *Desalination* 222 (2008) 176–186. <https://doi.org/10.1016/j.desal.2007.01.147>.
- [7] T. Younos, K.E. Tulou, Overview of desalination techniques: Overview of techniques, *J. Contemp. Water Res. Educ.* 132 (2009) 3–10. <https://doi.org/10.1111/j.1936-704X.2005.mp132001002.x>.
- [8] H. Fakharian, H. Ganji, A. Naderifar, Desalination of high salinity produced water using natural gas hydrate, *J. Taiwan Inst. Chem. E.* 72 (2017) 157–162. <https://doi.org/10.1016/j.jtice.2017.01.025>.
- [9] S. Ho-Van, B. Bouillot, J. Douzet, S.M. Babakhani, J.M. Herri, Cyclopentane hydrates – A candidate for desalination? *J. Environ. Chem. Eng.* 7 (2019) 103359. <https://doi.org/10.1016/j.jece.2019.103359>.
- [10] P. Gayet, C. Dicharry, G. Marion, A. Graciaa, J. Lachaise, A. Nesterov, Experimental determination of methane hydrate dissociation curve up to 55MPa by using a small amount of surfactant as hydrate promoter, *Chem. Eng. Sci.* 60 (2005) 5751–5758. <https://doi.org/10.1016/j.ces.2005.04.069>.
- [11] B. Mottet, inventor; BGH[FR], applicant. Method for crystallising clathrate hydrates, and method for purifying an aqueous liquid using the clathrate hydrates thus crystallised;

EP3153606, <https://worldwide.espacenet.com/patent/search/family/054476876/publication/WO2017060456A1?q=PCT%2FEF2016%2F074044>.

- [12] J. Zheng, M. Yang, Y. Liu, D. Wang, Y. Song, Effects of cyclopentane on CO₂ hydrate formation and dissociation as a co-guest molecule for desalination, *J. Chem. Thermodyn.* 104 (2017) 9–15. <https://doi.org/10.1016/j.jct.2016.09.006>.
- [13] S. Han, Y.W. Rhee, S.P. Kang, Investigation of salt removal using cyclopentane hydrate formation and washing treatment for seawater desalination, *Desalination* 404 (2017) 132–137. <https://doi.org/10.1016/j.desal.2016.11.016>.
- [14] S. Han, J.Y. Shin, Y.W. Rhee, S.P. Kang, Enhanced efficiency of salt removal from brine for cyclopentane hydrates by washing, centrifuging, and sweating, *Desalination* 354 (2014) 17–22. <https://doi.org/10.1016/j.desal.2014.09.023>.
- [15] D. Corak, T. Barth, S. Høiland, T. Skodvin, R. Larsen, T. Skjetne, Effect of subcooling and amount of hydrate former on formation of cyclopentane hydrates in brine, *Desalination* 278 (2011) 268–74. <https://doi.org/10.1016/j.desal.2011.05.035>.
- [16] F. Li, Z. Chen, H. Dong, C. Shi, B. Wang, L. Yang, Z. Ling, Promotion effect of graphite on cyclopentane hydrate based desalination, *Desalination* 445 (2018) 197–203. <https://doi.org/10.1016/j.desal.2018.08.011>.
- [17] Z. Ling, C. Shi, F. Li, Y. Fu, J. Zhao, H. Dong, Desalination and Li⁺ enrichment via formation of cyclopentane hydrate, *Sep. Purif. Technol.* 231 2020 115921. <https://doi.org/10.1016/j.seppur.2019.115921>.
- [18] S.M. Babakhani, S. Ho-Van, B. Bouillot, J. Douzet, J-M. Herri. Phase equilibrium measurements and modelling of mixed cyclopentane and carbon dioxide hydrates in presence of salts, *Chem. Eng. Sci.* 214 (2020) 115442. <https://doi.org/10.1016/j.ces.2019.115442>.

- [19] P. Linga, M.A. Clarke, A Review of reactor designs and materials employed for increasing the rate of gas hydrate formation, *Energ. Fuel* 31 (2017) 1–13. <https://doi.org/10.1021/acs.energyfuels.6b02304>.
- [20] S. Baek, J. Min, J.W. Lee, Inhibition effects of activated carbon particles on gas hydrate formation at oil-water interfaces, *RSC Adv.* 5 (2015) 58813–58820. <https://doi.org/10.1039/c5ra08335d>.
- [21] P. Babu, D. Yee, P. Linga, A. Palmer, B.C. Khoo, T.S. Tan, P. Rangsunvigit, Morphology of methane hydrate formation in porous media, *Energ. Fuel* 27 (2013) 3364–3372. <https://doi.org/10.1021/ef4004818>.
- [22] A. Siangsai, P. Rangsunvigit, B. Kitiyanan, S. Kulprathipanja, P. Linga, Investigation on the roles of activated carbon particle sizes on methane hydrate formation and dissociation, *Chem. Eng. Sci.* 126 (2015) 383–389. <https://doi.org/10.1016/j.ces.2014.12.047>.
- [23] A. Siangsai, P. Rangsunvigit, B. Kitiyanan, S. Kulprathipanja, Improved methane hydrate formation rate using treated activated carbon and tetrahydrofuran, *J. Chem. Eng. Jpn* 47 (2014) 352–357. <https://doi.org/10.1252/jcej.13we206>.
- [24] L. Yan, G. Chen, W. Pang, J. Liu, Experimental and modeling study on hydrate formation in wet activated carbon, *J. Phys. Chem. B* 109 (2005) 6025–6030. <https://doi.org/10.1021/jp045679y>.
- [25] S. Ho-Van, J. Douzet, B. Bouillot, J.M. Herri, Experimental study and modelling of cyclopentane hydrates in the presence of NaCl, KCl and a mixture of NaCl -KCl, 9th International Conference on Gas Hydrates - ICGH9, Jun 2017, Denver, USA
- [26] M. Kishimoto, S. Iijima, R. Ohmura, Crystal growth of clathrate hydrate at the interface between seawater and hydrophobic-guest liquid: effect of elevated salt concentration, *Ind. Eng. Chem. Res.* 51 (2012) 5224–5229. <https://doi.org/10.1021/ie202785z>.

- [27] G. Zylyftari, J.W. Lee, J.F. Morris, Salt effects on thermodynamic and rheological properties of hydrate forming emulsions, *Chem. Eng. Sci.* 95 (2013) 148–160. <https://doi.org/10.1016/j.ces.2013.02.056>.
- [28] H. Delroisse, J.P. Torr , C. Dicharry, Effect of a hydrophilic cationic surfactant on cyclopentane hydrate crystal growth at the water/cyclopentane interface, *Cryst. Growth Des.* 17 (2017) 5098–5107. <https://doi.org/10.1021/acs.cgd.7b00241>.
- [29] B. Tohidi, R.W. Burgass, A. Danesh, K.K. Østergaard, A.C. Todd, Improving the accuracy of gas hydrate dissociation point measurements, *Ann. NY Acad. Sci.* 912 (2000) 924–931. <https://doi.org/10.1111/j.1749-6632.2000.tb06846.x>.
- [30] R. Cohen-Adad, J.W. Lorimer, *Alkali Metal and Ammonium Chlorides in Water and Heavy Water (Binary Systems)*, Pergamon Press, 1991.